THE CORROSION BEHAVIORS OF FE-MN-AL-C ALLOYS

BY

JEN-LANG LUE

Submitted in Partial Fulfillment of the Requirements

for the Degree of

Master of Science

in the

Materials Science

Program

Richard W. Jones — June 5, 1990

Advisor — Date

Sally M. Hotchkiss — June 5, 1990

Dean of the Graduate School — Date

YOUNGSTOWN STATE UNIVERSITY

June, 1990

4-10-4

ABSTRACT

THE CORROSION BEHAVIORS OF FE-MN-AL-C ALLOYS

Jen-Lang Lue

Master of Science in Engineering

Youngstown State University, 1990

Three Fe-Mn-Al-C alloys with different Al contents and different structures are studied in potentiostatic corrosion tests and immersion tests in 30 ppm and 100 ppm NaCl solutions. The single phase (r) alloy has better corrosion behavior than do the dual phase alloys (r+α) regardless of the Al content. Also, as the α/r ratio in the microstructure increases, the corrosion resistance decreases.

ACKNOWLEDGEMENTS

The author wishes to thank his adviser, Dr. Richard W. Jones, Director of the Materials Science Program, for his continuous guidance, help, and noteworthy amount of time.

The author also wishes to thank Dr. C. M. Wan for offering these alloys and Famcy Steel Co., especially Mr. C. T. Lin.

TABLE OF CONTENTS

LIST OF TABLES

LIST OF FIGURES

CHARPTER I

INTRODUCTION

Several previous research studies indicate Fe-Mn-Al-C alloys are good candidates to substitute for some of the conventional austenitic Ni-Cr stainless steels due to their significant cost and density advantages, excellent mechanical properties, and promising corrosion and oxidation resistance. The significant cost and density advantages of these alloys are because Mn and Al are both less expensive and lighter than Ni and Cr. By replacing Cr with Al, the Fe-Al based alloys can have a lower density with an excellent oxidation and corrosion resistance. However, due to their ferritic structures, these alloys are usually very brittle and have poor high-temperature strength. Since Mn and C can stabilize the austenite (r) loop, the Fe-Al-Mn alloys have the potential for retaining the austenitic structure (F.C.C.) with possibly better workability and high-temperature oxidation resistance [1,2,3]. Hence, a suitable well-organized combination of Al, Mn, and C should give an austenite alloy with good mechanical properties, while retaining the good oxidation resistance characteristic of Fe-Al alloys.

In the Fe-Al-Mn-C alloy, Mn and C are austenite stabilizers and Al is a ferrite stabilizer. The Mn necessary to produce a F.C.C. structure depends on the Al and C contents. In general, the amount of Mn should

increase with increasing Al or decreasing C content [4]. Based on G. L. Kayak's work [5], the Mn should not be lower than 23.7% and Al should not be greater than 10.2%; otherwise, the precipitation of Fe-Al carbide would cause a breakdown of the austenite structure. Thus, to keep a F.C.C. structure with good mechanical properties, a minimum amount of Mn is required for a given Al content.

In 1960, D. J. Schmatz [6] reported one promising composition range of 8-9Al, 30-35Mn, 0.75C 1-2Si, bal.Fe. He specifically recommended a composition of 8Al, 30Mn, 1C, 1.5Si, bal.Fe. Its strength exceeded that of commercial stainless steel in the quenched condition and increased by both quench aging and strain aging. The oxidation resistance of the 8Al-30Mn was somewhat inferior to an equivalent binary Fe-Al alloy, but with a "pre-oxidatizing" treatment its oxidation resistance was adequate to 1400°F. He also suggested that embrittlement in alloys with higher Al and Mn contents was probably caused by a transition to β-Mn structure.

In order to form a continuous protective film for oxidation resistance, the minimum Al in Fe-Al-Mn-C alloy is about 8% [2,3,7]. If the Al content is too high, a ferritic structure results which is not suitable for high-temperature applications. R. Wang and F. H. Beck [8] reported one promising composition Fe-30Mn-10Al-Si. This alloy has good resistance to marine corrosion and to cavitation erosion. It is used for seagoing ship

propellers and may be a substitute for conventional stainless steel without Ni or Cr. Recent research on the corrosion behavior of several Fe-Mn-Al austenite steel in aqueous environments has been reported by R.A. Rapp. et al. [8,9,10]. The corrosion behavior in a more aggressive or aqueous environment has not been completely studied in this alloy system and more corrosion work is required for these alloys.

A full austenite (r) phase of Fe-Mn-Al-C alloys always has high strength and high toughness [3,11], which gives the alloys poor machinability and requires higher forming forces than are usually required for conventional stainless steels. In most steel forming and fabrication industries, steels with low strength and high formability are required for economic reasons. In order to promote the Fe-Al-Mn-C alloys for such applications, an austenite-ferrite ($r+\alpha$) dual phase can be produced with lower strength and higher workability by adjusting the Mn-Al-C composition. Such an alloy would have the advantage of improved machining and forming characteristics. Also, it would have better resistance to both stress corrosion and hydrogen embrittlement [12].

The ($r+\alpha$) dual phase of Fe-Mn-Al-C based alloy system is not completely understood regarding mechanical properties, corrosion behavior, oxidation behavior and morphology. Thus, because of their potential industrial importance, and since Fe-Al-Mn-C alloys have not been

completely researched, they are good candidates for continued study. The present work is to study the effect of Al on the corrosion behavior of (r+α) dual phase alloys. In fully austenitic structures, the corrosion resistance increases with increasing Al content due to the increased Al_2O_3 passive surface film [13]. Al is a strong ferritic stabilizer; while the Al content is limited in an austenite structure, it produces a dual (r+α) structure and the α/r ratio is related to the Al content. The influence of Al on structure changes and corresponding changes in corrosion behavior is stressed in the present research.

The corrosion behavior is usually described by the concept of polarization curves and immersion tests. Fig. 1 schematically illustrates the typical polarization of an active-passive metal in an aggressive environment. The only point where the total rates of oxidation and reduction are equal is represented by a corrosion potential, E_{corr}. The current density corresponding to E_{corr} is usually called corrosion current density, I_{corr}. The maximum anodic current density, i.e., the critical anodic current density, I_c, is characterized by the primary passive potential, E_{pp}. In the active region, the dissolution rate increases exponentially. In the passive region, the dissolution rate decreases to a very small value and remains essentially independent of potential over a considerable potential range. Finally, at very noble potentials, dissolution rate again increases with

increasing potential in the transpassive region; i.e., where passive and active states coexist. The breakdown potential, E_b, is the point where the system changes from a passive to a transpassive region where metals exhibit pitting corrosion. Therefore, E_b can be considered as a measure of the susceptibility of different metals and alloys to pitting corrosion in aggressive environments. The influence of different factors, e.g., steel composition, concentration of solution, temperature of solution, heat treatment, etc., can be characterized by the determination of E_b. The purpose of the immersion test is simply to measure weight loss and calculate a corrosion rate. It is more accurate because there are fewer apparatus errors. From the polarization curves and immersion tests, we can investigate the corrosion behavior of different compositions. Presented here are the polarization curves and immersion results for three different Fe-Al-Mn-C alloys.

CHARPTER II

EXPERIMENTAL PROCEDURE

2.1 MATERIAL PREPARATION:

All three alloys were prepared by use of a laboratory induction furnace. Table I shows the chemical composition of these alloys.

The following treatments (Fig. 2) were adopted to process the materials after casting: homogenization at 1100 °C for 3 hrs, hot forging at 1200 °C (about 80% reduction in thickness), air cooled, and then followed by a solution treatment at 1100 °C for 1.5 hrs, then air cooled once more. All the materials were then cold rolled to 2 mm in thickness and were cut into 100 mm x 10 mm x 2 mm sheets in the longitudinal direction. Finally, all the materials were treated in a ceramic tube furnace at 1050 °C for 2 hrs with flowing argon which prevented high-temperature oxidation to obtain a suitable grain size and then water quenched.

2.2 CYCLIC POTENTIODYNAMIC POLARIZATION MEASUREMENT:

Two solutions were used in this study: 30 ppm and 100 ppm NaCl solutions. Samples A, B, and C (Table I) with a size of 15 mm x 10 mm x 2 mm were cut from the sheets. A 409 stainless steel was also studied in 100 ppm NaCl solution. A stainless wire covered with heat-shrinkage rubber tubing was welded to the back of the specimens for

electric connection to the potentiostat. The specimens then were mounted by epoxy resin and wet ground with 600 grit silicon carbide paper and cleaned ultrasonically in acetone. Microstop was used to give an exposed area of $1cm^2$ and also to prevent crevice corrosion.

The polarization apparatus used was an EG & G Princeton Applied Research including Model 273 Potentiostat and IBM PC with Model 342 software to perform computer-controlled electrochemical measurements. The volume of solution was 0.8 liter. Before polarization measurements, the NaCl solution was deaerated with purified nitrogen bubbling for one hour prior to and during the corrosion test in a glass cell, which is shown in Fig. 3. The polarization measurements were performed in this glass cell. A graphite rod was used as the counter electrode. All potentials were measured with respect to a saturated calomel electrode (SCE) connected to the cell. The polarization experiment was scanned from -1300 mv to 500 mv by scanning at a rate of 1 mv/sec. All the potential records, current density and polarization curves were recorded with the IBM computer.

2.3 POTENTIAL-TIME PLOTS:

The experimental procedure was the same as the cyclic potentiodynamic polarization measurement except that it did not use a counter electrode and the testing cell was exposed to air. The open circuit corrosion potential was

2.6 X-RAY STUDY:

The phase structures of these three alloys were investigated and identified by an X-ray diffraction technique. X-ray patterns were run at room temperature on a Philips Powder Diffractometer by using a copper target ($CuK\alpha$, λ = 1.5405 Å). A standard quartz was used to calibrate the diffractometer.

2.7 ENERGY-DISPERSIVE SPECTROMETRY (EDS):

A qualitative chemical analysis of each phase was obtained by using a scanning electronic microscope (Model JEOL JSM35C) equipped with an energy dispersive x-ray spectrum analyzer (EDAX).

CHAPTER III

RESULTS

3.1 MICROSTRUCTURES AND X-RAY STUDIES:

Figs. 4 through 6 show the microstructures of the three alloys A, B, and C before potentiodynamic polarization tests. From X-ray studies, alloy A was a fully austenitic structure; alloy B and alloy C were dual phase (austenite + ferrite) structures. The austenitic microstructure for alloy A is shown in Fig. 4. Fig. 5 shows the dual phase structure for alloy B in which the long island-like shapes are ferrites. Fig. 6 shows the dual phase structure of alloy C. These three figures show that the ferrite phase increases with increasing Al content. Alloy C has more ferrite than alloy B. Alloy B is about 30% ferrite and alloy C is about 50% ferrite. Figs. 7 through 9 show the surface conditions of the three alloys after potentiodynamic polarization. Pittings occur on all three alloys. Fig. 10 shows the microstructure of alloy B which was etched after potentiodynamic polarization; the greatest pitting occurs in the ferrite phase regions.

3.2 CYCLIC POTENTIODYNAMIC POLARIZATION CURVES:

The potentiodynamic polarization curves of alloys A, B, and C in 30 ppm and 100 ppm NaCl solutions and 409 stainless steel are plotted in Figs. 11 through 17. Figs. 11 through 16 reveal that these alloys A, B, and C do not

show the expected passive plateaus. Fig. 17 reveals that 409 stainless steel still has an apparent passive plateau. Tables II & III list the potentiodynamic polarization values E_b, E_{pp}, E_{corr}, I_b, I_{pp}, I_{corr} measured from the polarization curves for each alloy. The comparisons of breakdown potentials of alloys A, B, and C and 409 stainless steel in each solution are illustrated in Figs. 18 through 21. Alloy A has the highest breakdown potential, which is 25 mv in 30 ppm NaCl solution and -38 mv in 100 NaCl solution; alloy C has the lowest breakdown potential, which is -35 mv in 30 ppm NaCl solution and -355 mv in 100 ppm NaCl solution. The breakdown potential for alloy B is -23 mv in 30 ppm Nacl solution and -227 mv in 100 ppm NaCl solution. The breakdown potential in 100 ppm NaCl solution is lower than in 30 ppm Nacl solution for alloys A, B, and C. The breakdown potential of 409 stainless steel in 100 ppm NaCl solution was 650 mv and is higher than these three alloys in each solution. The potential versus time curve in open circuit is shown in Fig. 22. The potentials of these three alloys apparently change with time. None of the alloys shows a constant potential with time.

3.3 IMMERSION TEST:

Table IV lists the corrosion rate (R_W) of alloys A, B, and C from weight-loss data in each solution. The corrosion rates in terms of millimeters per year (mm/yr) were easily calculated from weight-loss data by using the following equation:

$$R_W = \frac{87600 \times W}{D \times A \times T}$$

where

R_W = the corrosion rate in mm/yr

W = the weight loss of specimen in grams

D = the density of alloys in g/cm^3

A = the surface area in cm^2

T = the time of immersion in hours

The comparisons of the corrosion rates of alloys A, B, and C in each solution are shown in Figs. 23. Alloy A has the slowest corrosion rate, which is 0.0124 mm/yr in 30 ppm NaCl solution and 0.0151 mm/yr in 100 ppm NaCl solution; alloy C has the fastest corrosion rate, which is 0.0158 mm/yr in 30 ppm NaCl solution and 0.0168 mm/yr in 100 ppm NaCl solution. The corrosion rate for alloy B is 0.0149 mm/yr in 30 ppm NaCl solution and 0.0159 mm/yr in 100 ppm NaCl solution. The corrosion rate in 100 ppm NaCl solution is faster than in 30 ppm NaCl solution for each alloy as expected.

3.4 EDAX ANALYSES:

Figs. 24 through 27 show the EDAX analyses for alloy B and alloy C for the austenite and ferrite phases. Clearly, from the peak intensity the Al content in each phase is different. The ferrite phase has more Al content than does the austenite phase.

CHAPTER IV

DISCUSSION

None of the three alloys exhibits an obvious passive plateau in its polarization curve (Figs.11-16). Also, the open-circuit corrosion curve shows that the corrosion potential changed with time. There should be a constant potential with time for good corrosion resistance in an aggressive environment. Also, the E_b of alloys A, B, and C is much lower than that of 409 stainless steel in 100 ppm NaCl solution. So, it is shown that these three alloys did not have good corrosion resistance in either 30 ppm or 100 ppm NaCl solution. This was also proved by immersion tests. With 304 stainless steel the corrosion rate is approximately zero in a 3.5% NaCl solution, which is more aggressive than a 100 ppm NaCl solution [17]. The corrosion rates in 30 and 100 ppm NaCl solutions range from 0.012-0.018 mm/yr. The corrosion rate in a low concentration NaCl solution should be zero for good corrosion resistance materials. It was evident that there is not good corrosion resistance in these alloys.

The potentiodynamic polarization curves and immersion test data show that the increase of Al content has the effect of increasing the corrosion rate. The corrosion rate in the 100 ppm NaCl solution was faster than in the 30 ppm NaCl solution because the Cl^- ions attacked the Fe^{2+} ions. The faster corrosion rate in the more concentrated

NaCl solution was expected because there were more Cl^- ions. As the Al content increased, the microstructure changed from austenite (F.C.C.) to austenite plus ferrite (F.C.C. + B.C.C.), and the fraction of ferrite increased with increasing Al content. As the ferrite precipitated, it formed a local galvanic cell with austenite. From EDAX analyses the ferrite phase has a different composition from the austenite phase. A potential difference existed between ferrite and austenite when it was immersed in a corrosive or conductive solution, such as NaCl solution. This potential difference produced an electron flow between the phases which accelerated the corrosion rate. The exact potential difference between austenite and ferrite was not determined in this experiment and further study is needed. The more resistant austenite phase is cathodic and the less resistant ferrite is anodic. The cathode-anode of dual phases is proved by the Fig. 10. Large pittings occur in the ferrite phase due to its anodic potential resulting from an oxidation reaction. The total potential difference in each alloy is due to the sum of the all potentials for all the galvanic cells in the alloy in series. Therefore, alloy C had a greater potential difference than alloy B because there are more cells in alloy C. The driving force for current and corrosion was the potential developed between ferrite and austenite. Thus, alloy C has the fastest corrosion rate. In a fully austenitic structure, the corrosion resistance in NaCl solution increases with

increasing Al content due to its more Al_2O_3 passive films. Although alloy B and alloy C have more Al than does alloy A, they still have poorer corrosion resistance than alloy A. This can be explained by 1) the structure changes as the Al content increases, and 2) the structure is not totally austenitic. This means that structure, not composition, controls the relative corrosion rates of the two phases in these alloys. From the EDAX analyses the Al content of the ferrite phase is greater than the Al content of the austenite phase. However, because the ferrite acted as an anode in the electrochemical cell established between the two phases, it corroded faster than did the austenite phase. The ferrite phases had greater pitting corrosion than did the austenite phase despite the fact it contained more aluminum. This demonstrates that Al content alone is not sufficient to prevent corrosion when the structure changes from a single austenite to a dual austenite + ferrite phase structure. Thus, structure is more important than composition in these alloys.

CHAPTER V

CONCLUSION

1. These three alloys do not have good resistance in 30 ppm NaCl solution or 100 ppm NaCl solution.

2. The corrosion rate in 100 ppm NaCl solution is faster than in 30 ppm NaCl solution for all alloys studied.

3. The ferrite phase has a faster corrosion rate than does austenite phase.

4. Dual phase alloys have worse corrosion resistance than a single phase alloy, even though the Al content increases. The corrosion resistance decreases with increasing ferrite which precipitates with increasing Al.

Table I Chemical Composition of Alloys (Wt%)

	Mn	Al	C	Fe	Structure
Alloy A	26.22	5.68	0.31	Bal.	Full r
Alloy B	25.69	7.53	0.29	Bal.	30% α
Alloy C	26.06	8.22	0.24	Bal.	50% α

Table II Potentiodynamic Polarization Properties in 100 ppm NaCl Solution

	E_{corr} (mv)	I_{corr} (ua/cm^2)	E_{pp} (mv)	I_c (ua/cm^2)	E_b (mv)	I_b (ua/cm^2)
A	-1004	$6.71x10^1$	-67	$5.13x10^2$	-38	$5.15x10^2$
B	-996	$2.63x10^1$	-315	$1.29x10^2$	-227	$7.1x10^1$
C	-1011	$3.41x10^1$	-447	$7.27x10^1$	-355	$5.09x10^1$

Table III Potentiodynamic Polarization Properties in 30 ppm NaCl Solution

	E_{corr} (mv)	I_{corr} (ua/cm^2)	E_{pp} (mv)	I_c (ua/cm^2)	E_b (mv)	I_b (ua/cm^2)
A	-943	$3.55x10^{1}$	-35	$1.17x10^{2}$	25	$1.10x10^{2}$
B	-795	$1.19x10^{1}$	-195	$6.61x10^{1}$	-23	$4.83x10^{1}$
C	-652	$1.4x10^{-1}$	-213	$6.05x10^{1}$	-35	$3.6x10^{1}$

Table IV Corrosion Rate Rw in Each Solution

	30 ppm (mm/yr)	100 ppm (mm/yr)
Alloy A	0.0124	0.0151
Alloy B	0.0149	0.0159
Alloy C	0.0158	0.0169

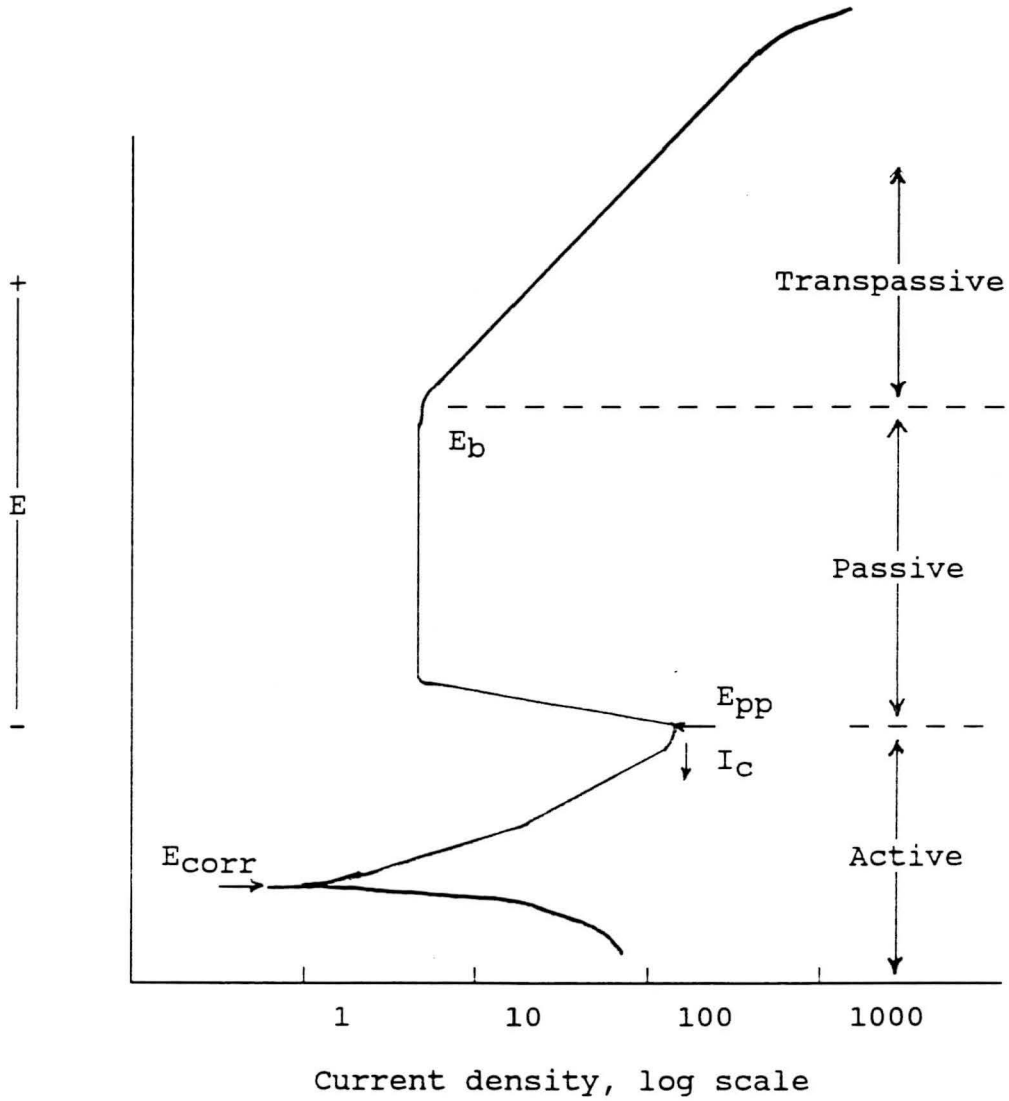

Fig. 1 Typical Polarization of an Active-passive Metal in an Aggressive Environment.

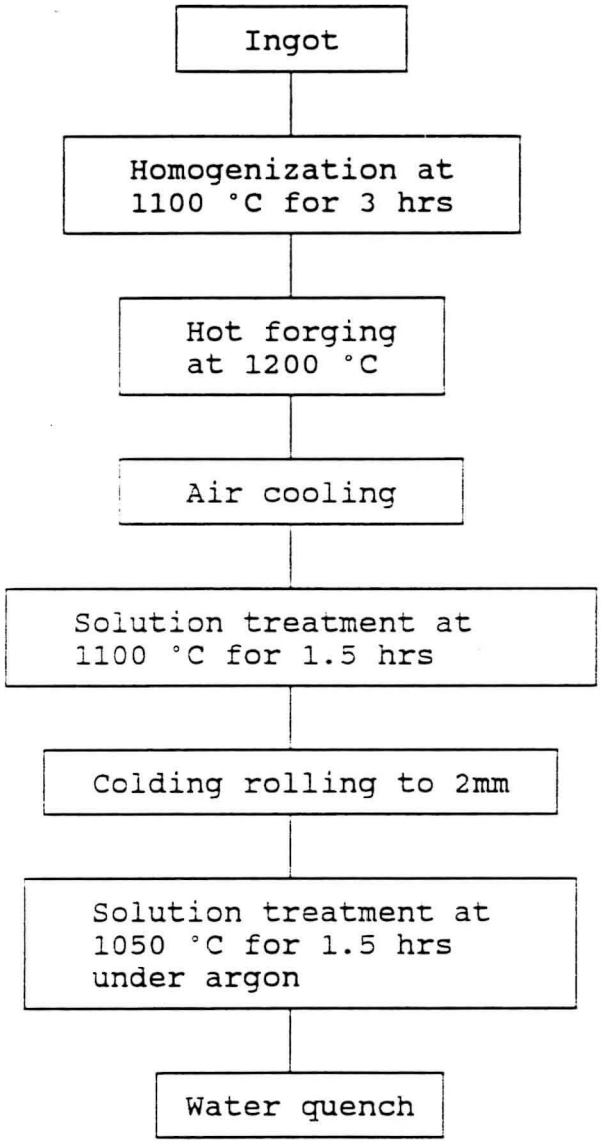

Fig. 2 Flow Chart of Materials Preparation

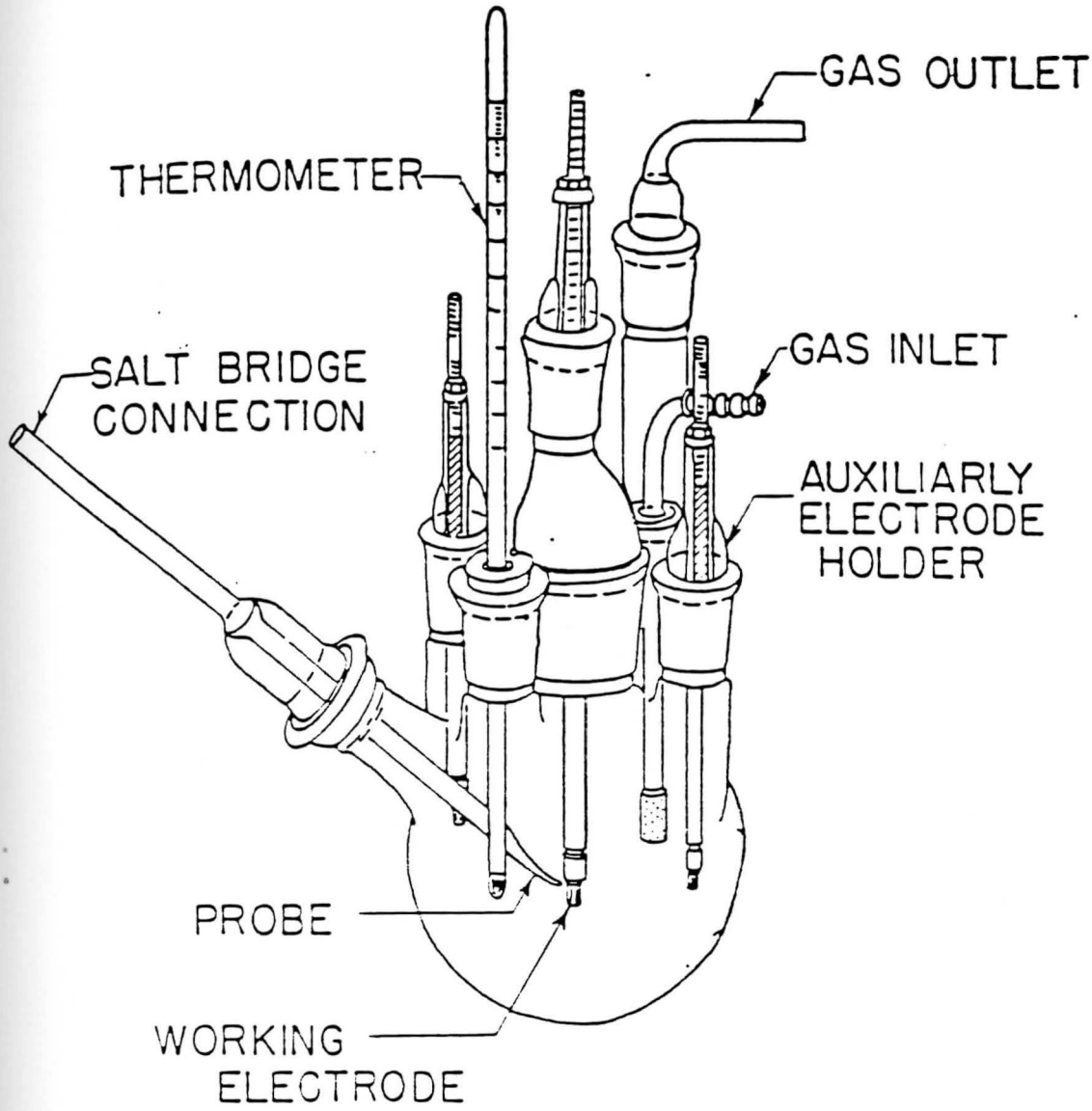

FIG. 3 Standard Polarization Cell Schematic Diagram

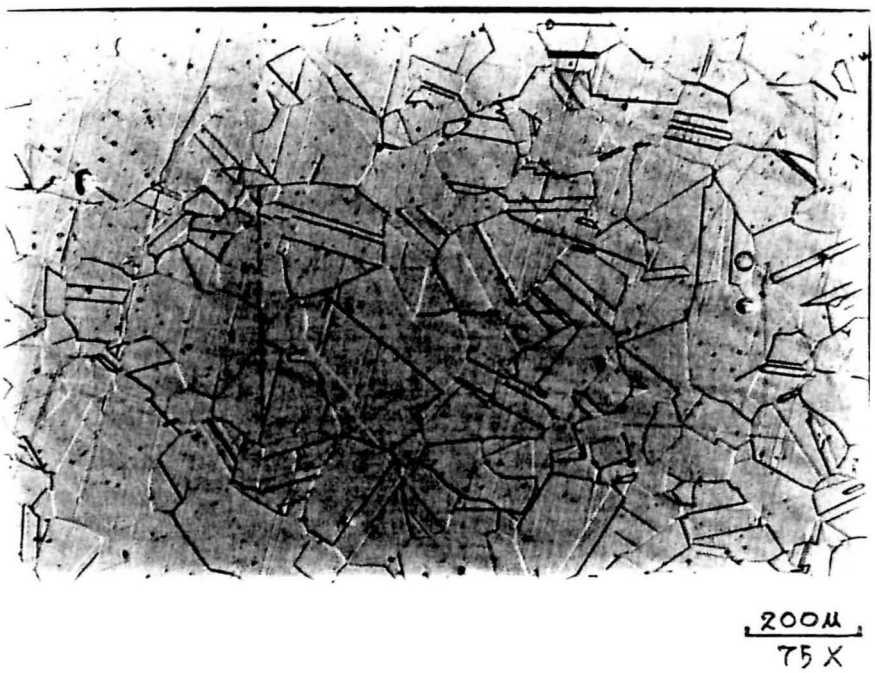

FIG. 4 OM Microstructure of Alloy A After Solution Treatment at 1050 °C for 1.5 hrs Under Argon.

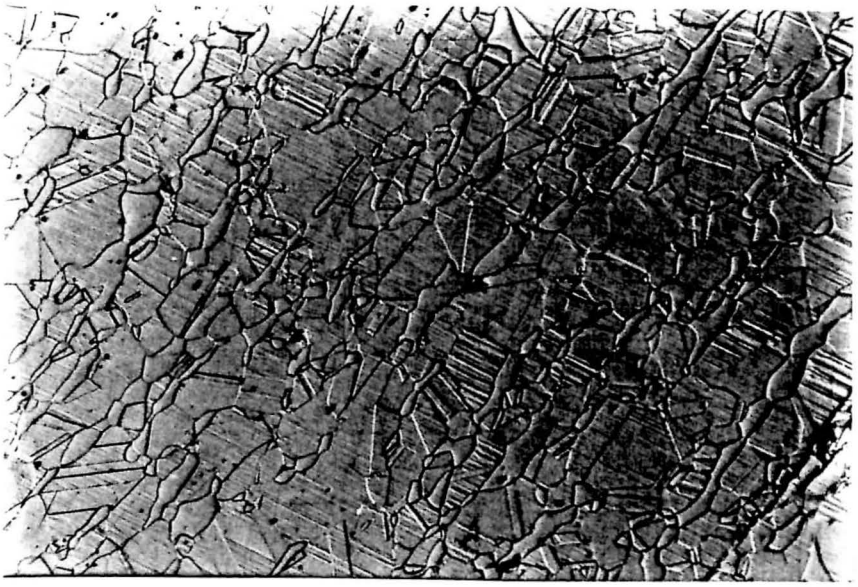

FIG. 5 OM Microstructure of Alloy B After Solution Treatment at 1050 °C for 1.5 hrs Under Argon.

100μ
75X

FIG. 6 OM Microstructure of Alloy C After Solution Treatment at 1050 °C for 1.5 hrs Under Argon.

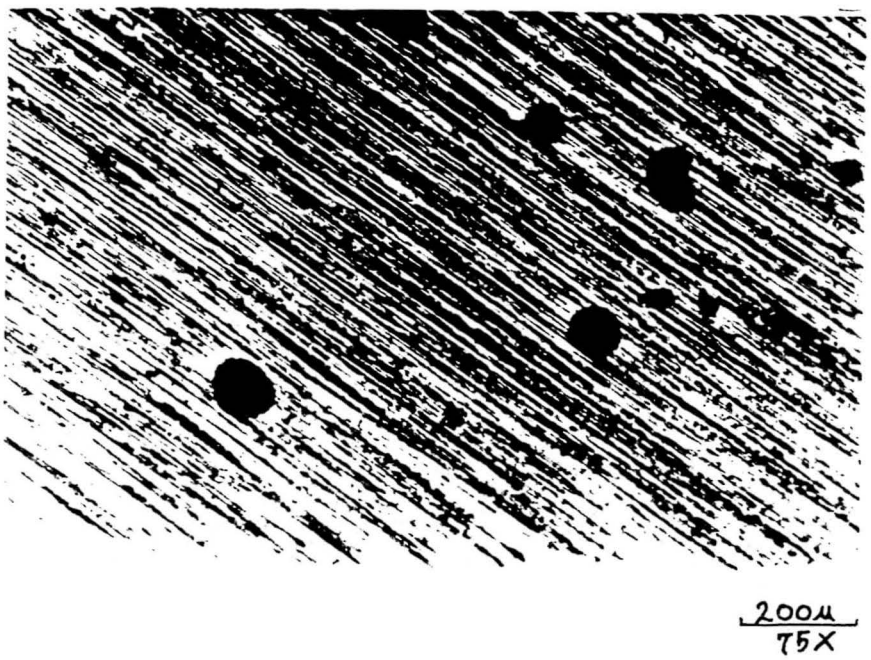

FIG. 7 The Morphology of Alloy A After Potentiodynamic Polarization in 100ppm NaCl Solution.

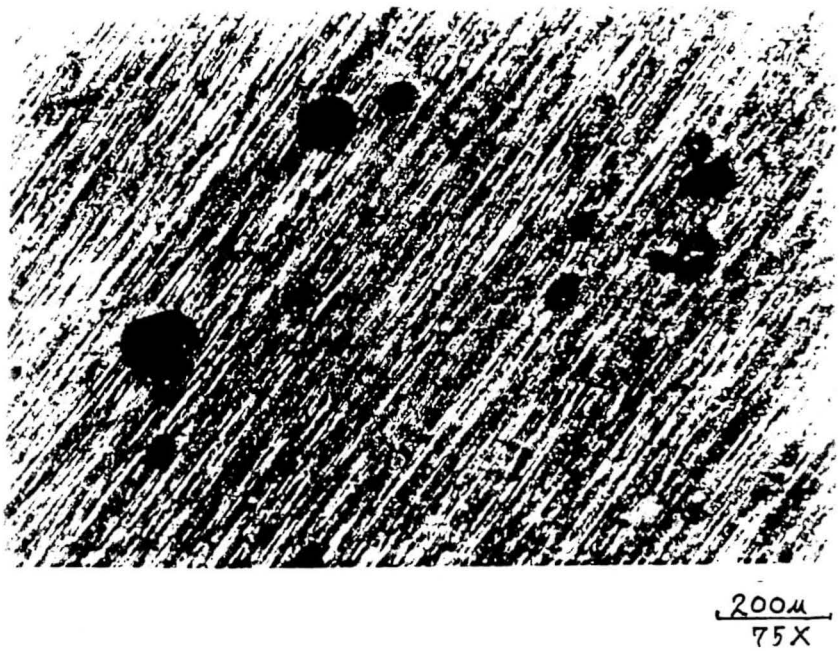

FIG. 8 The Morphology of Alloy B After Potentiodynamic Polarization in 100ppm NaCl Solution.

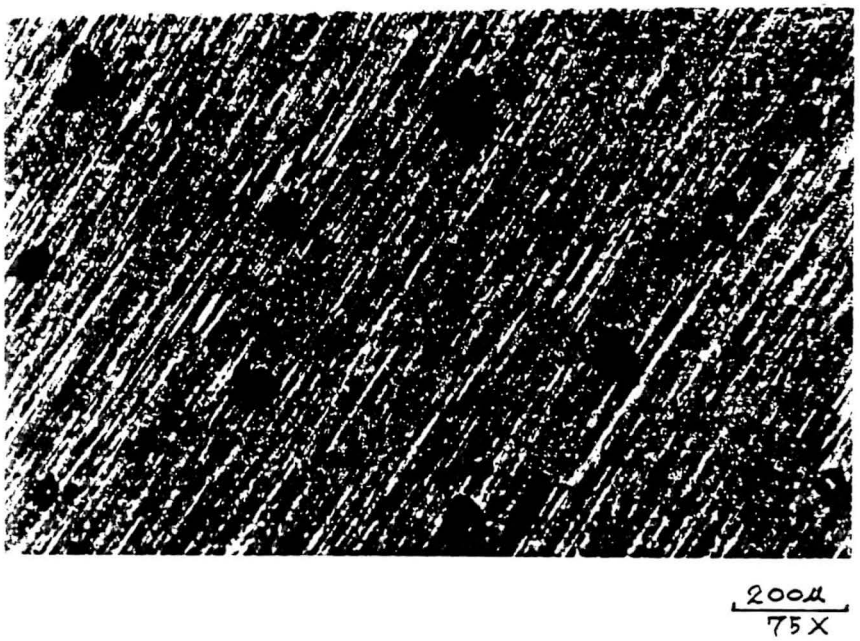

FIG. 9 The Morphology of Alloy C After Potentiodynamic Polarization in 100ppm NaCl Solution.

FIG. 10 The Morphology of Alloy B After Potentiodynamic Polarization in 100ppm NaCl Solution And Chemical Etching.

FIG.11 POTENTIAL VS CURRENT DENSITY

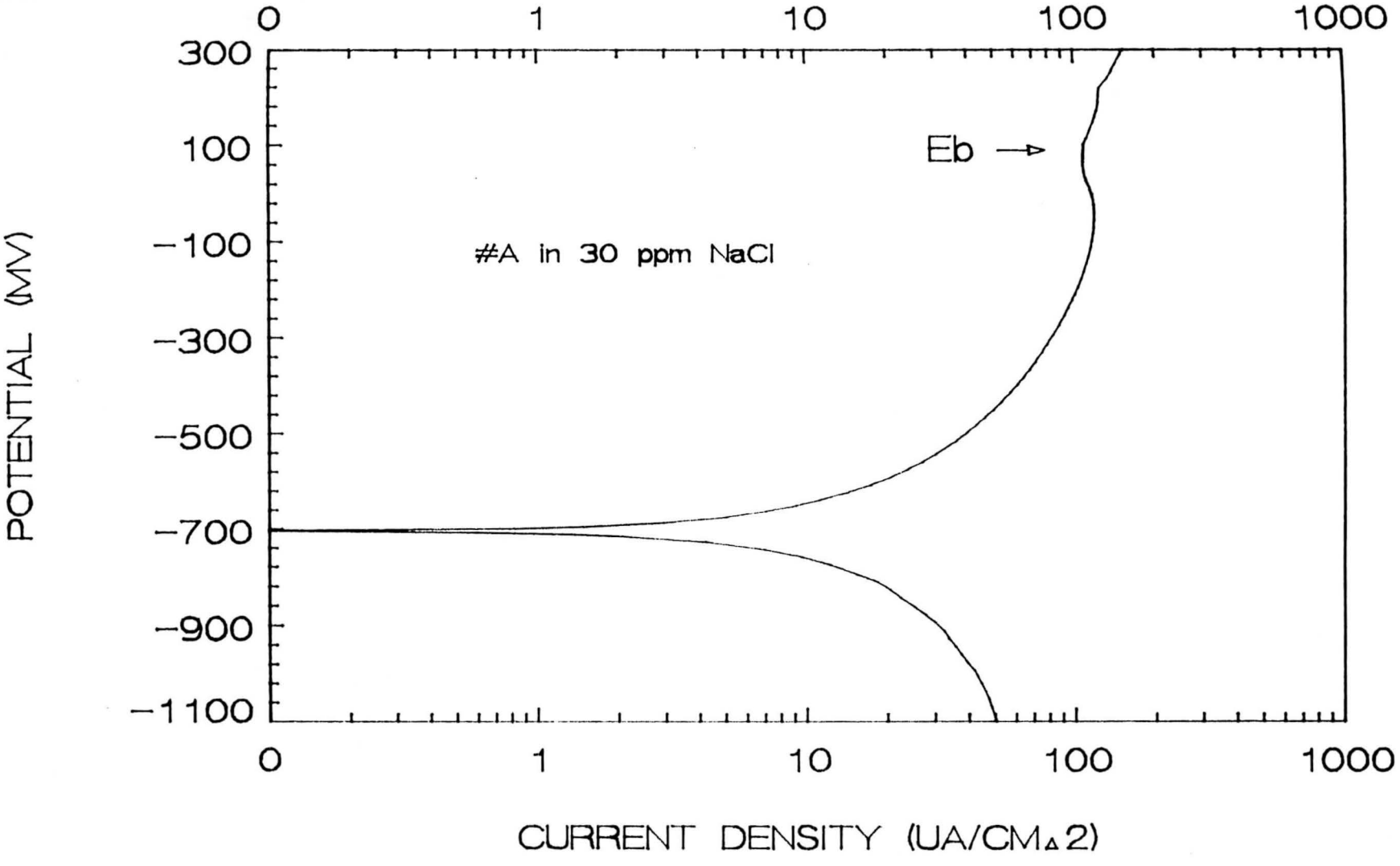

FIG.12 POTENTIAL VS CURRENT DENSITY

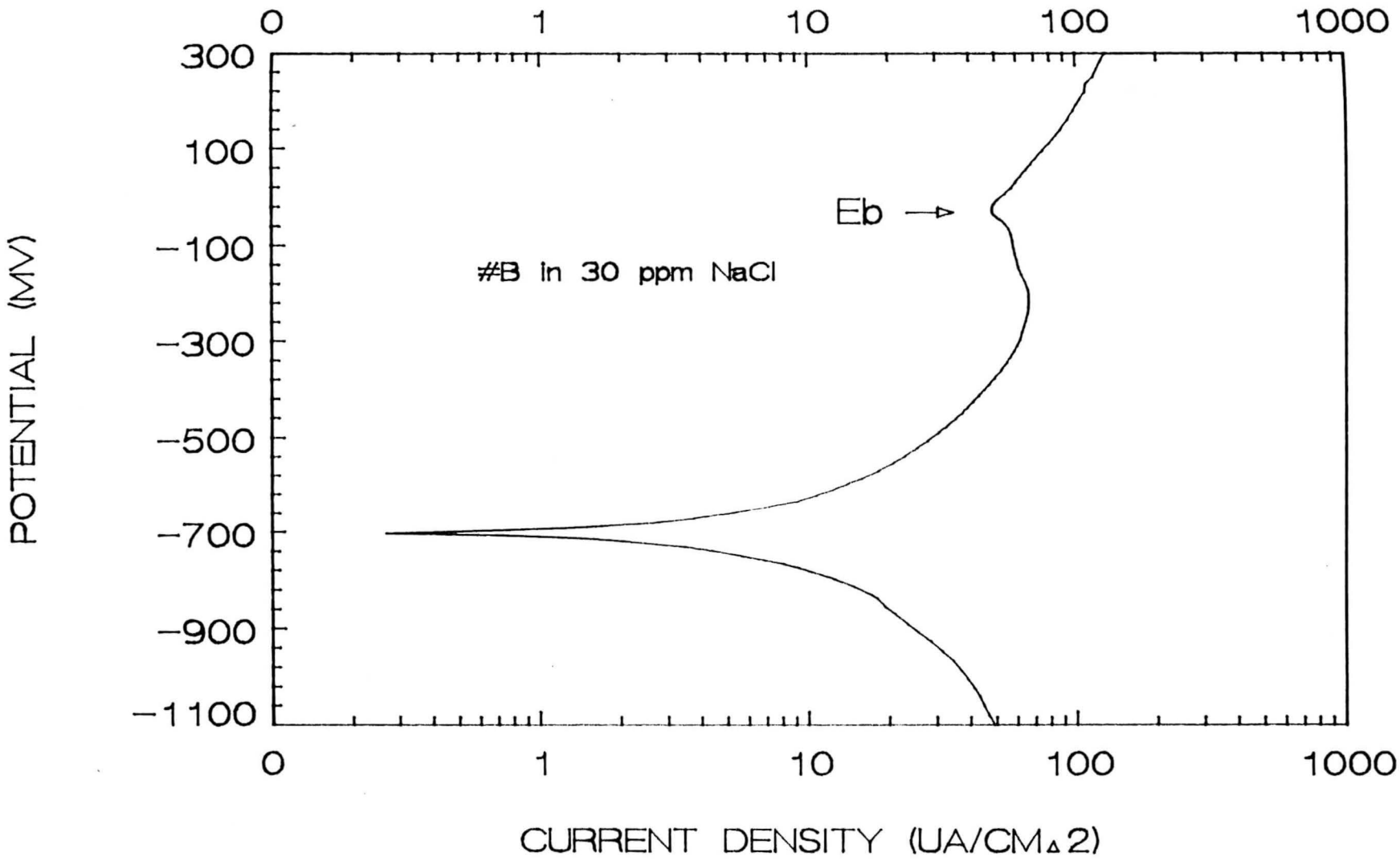

FIG.13 POTENTIAL VS CURRENT DENSITY

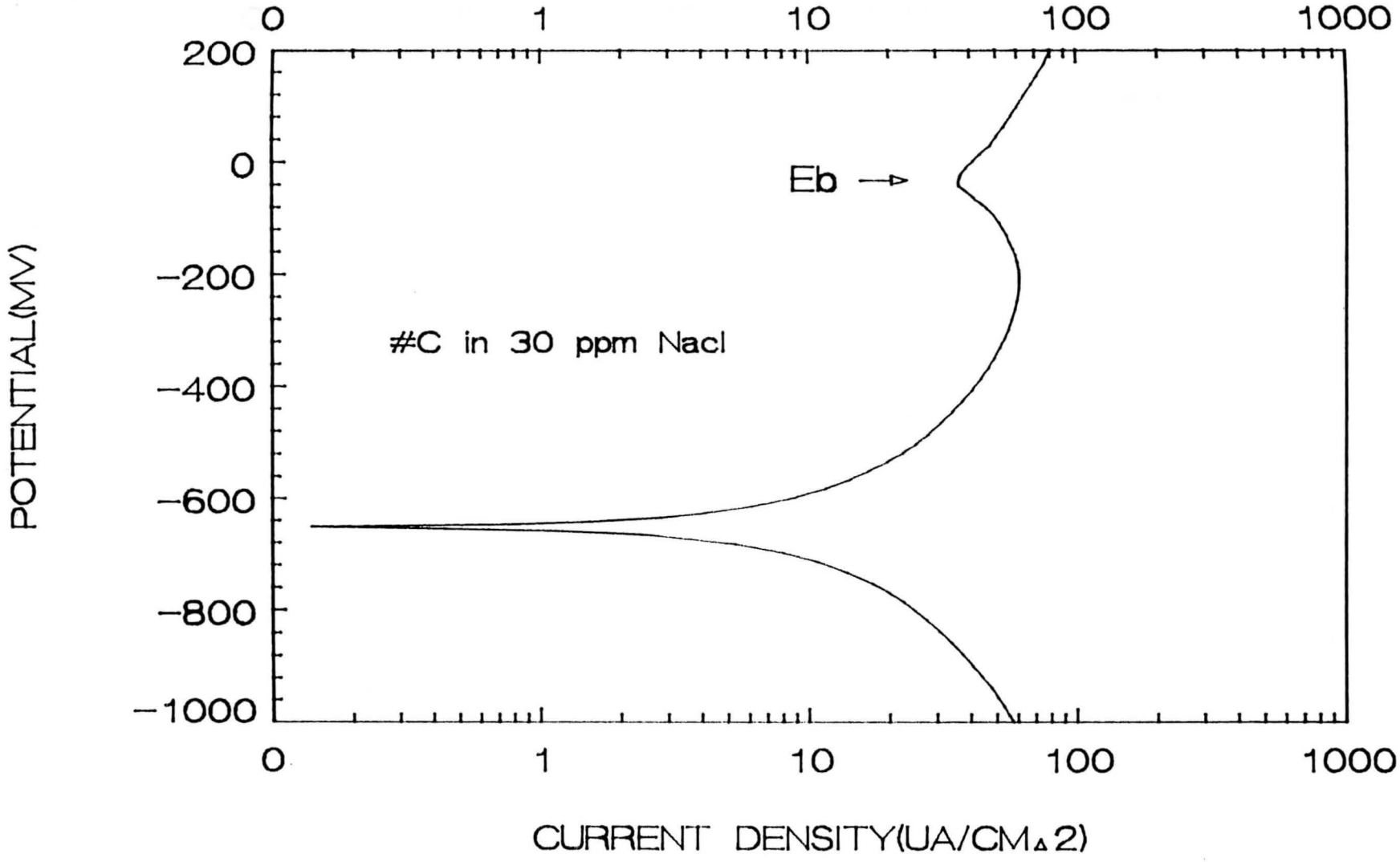

FIG.14 POTENTIAL VS CURRENT DENSITY

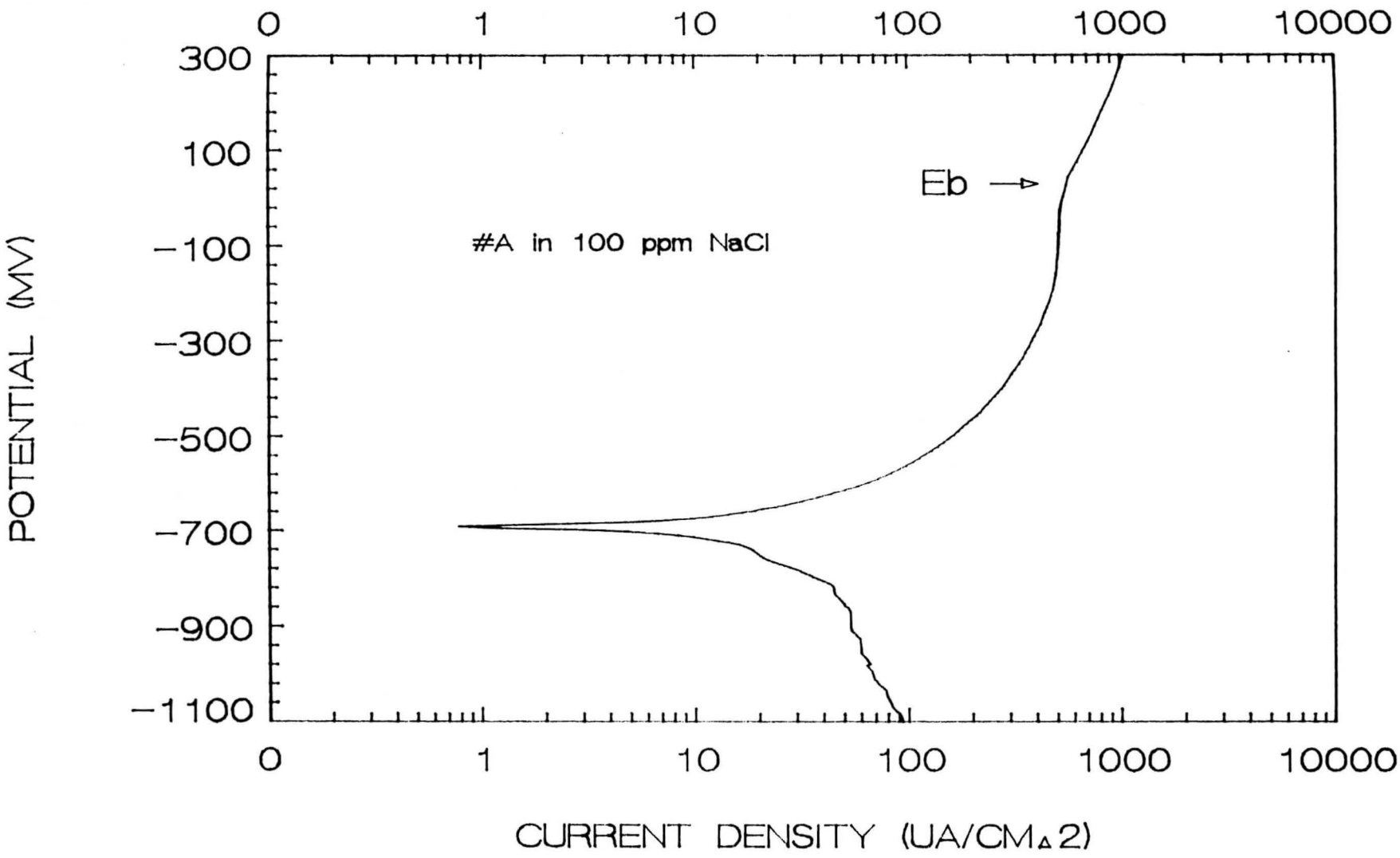

FIG.15 POTENTIAL VS CURRENT DENSITY

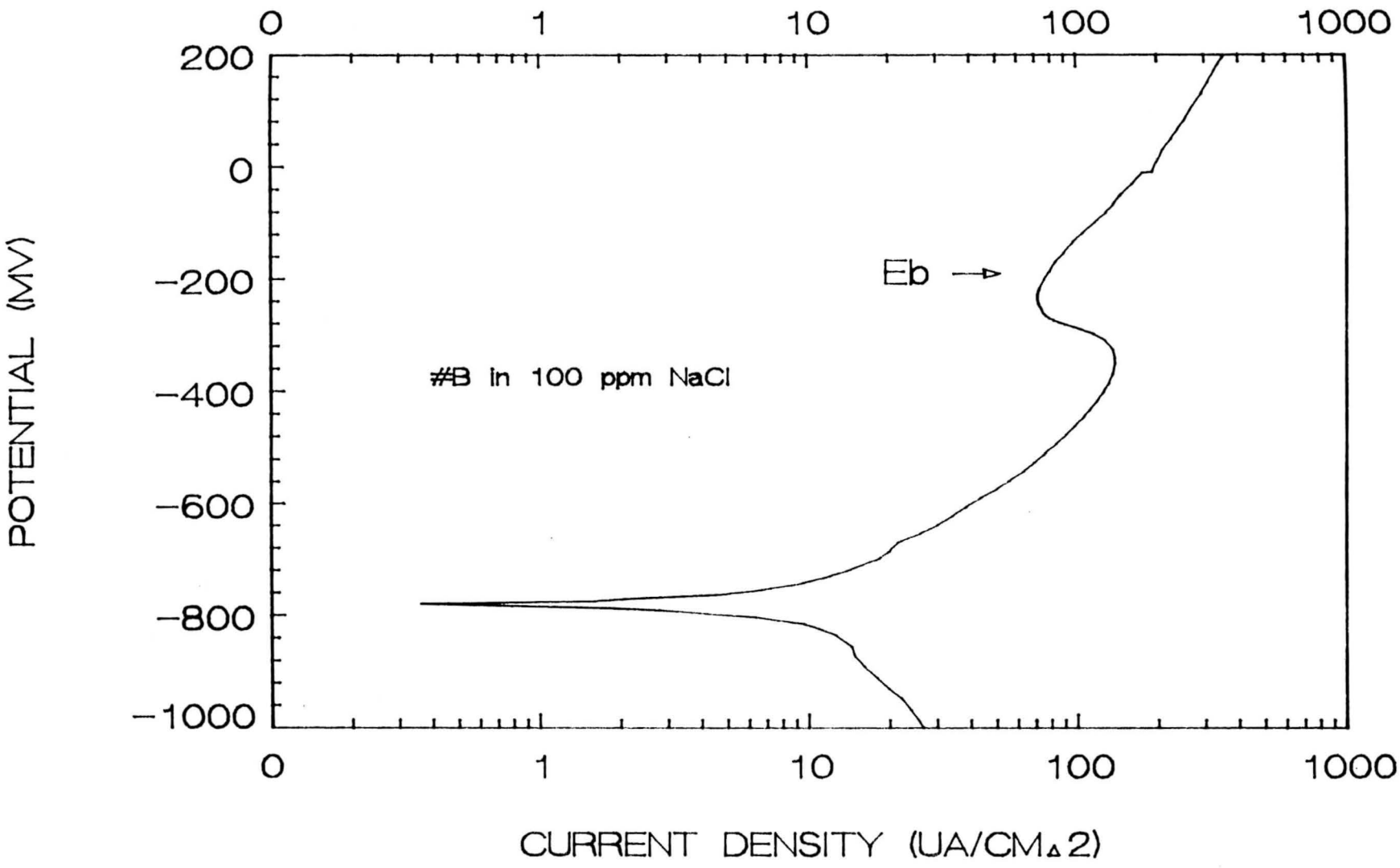

FIG.16 POTENTIAL VS CURRENT DENSITY

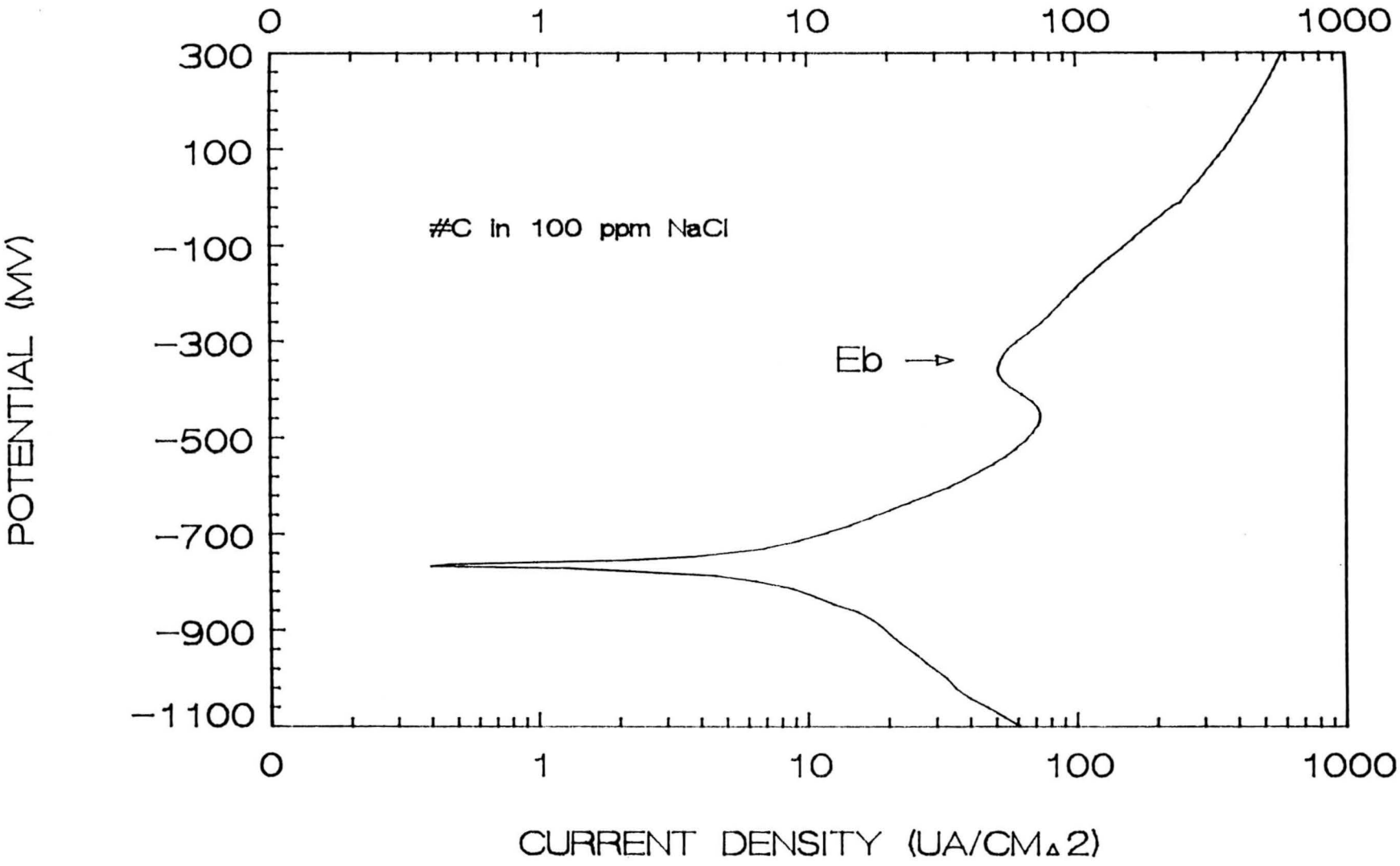

FIG.17 POTENTIAL VS CURRENT DENSITY

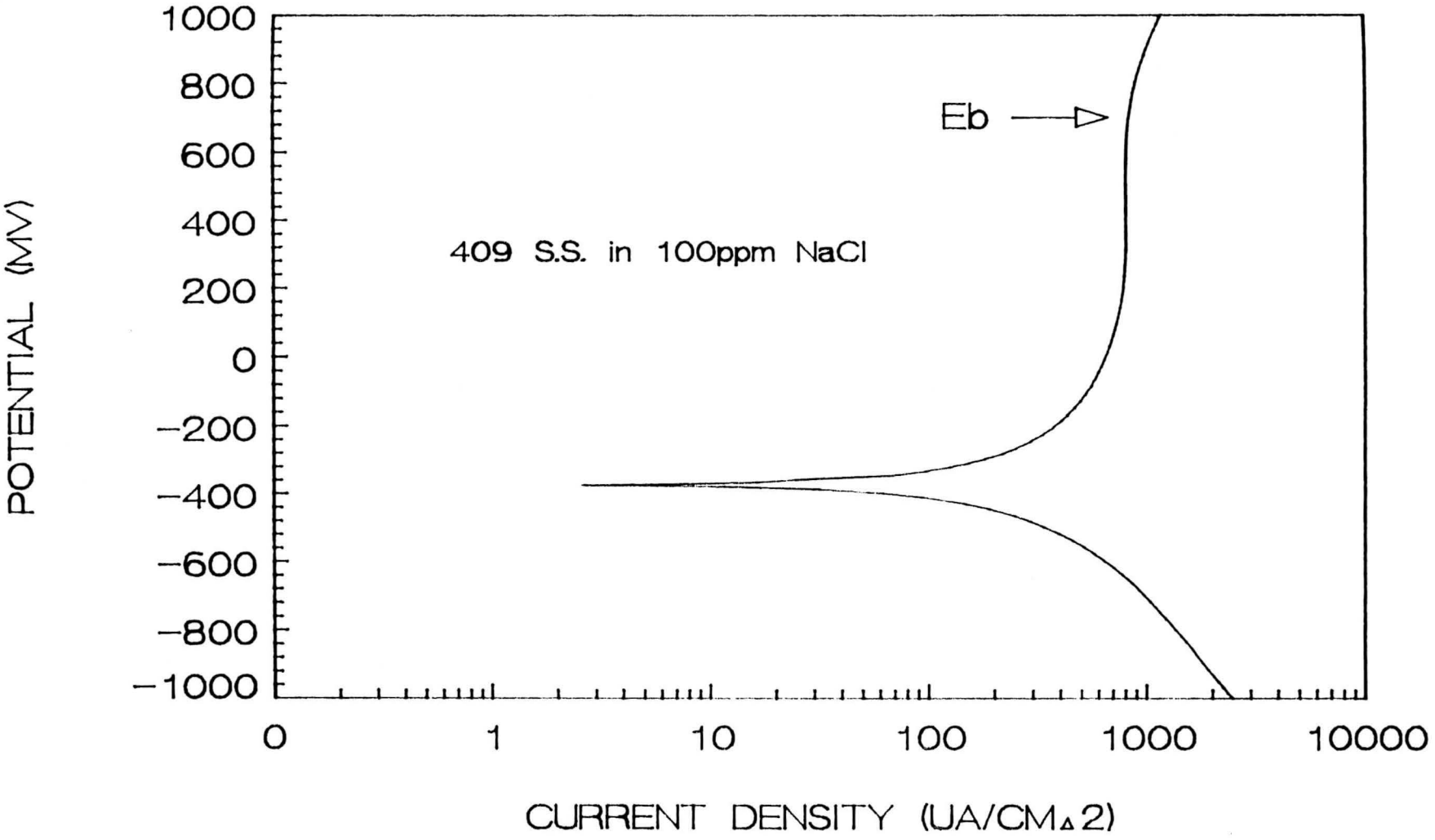

FIG.18 POTENTIAL VS. AL CONTENT
IN 30PPM NACL

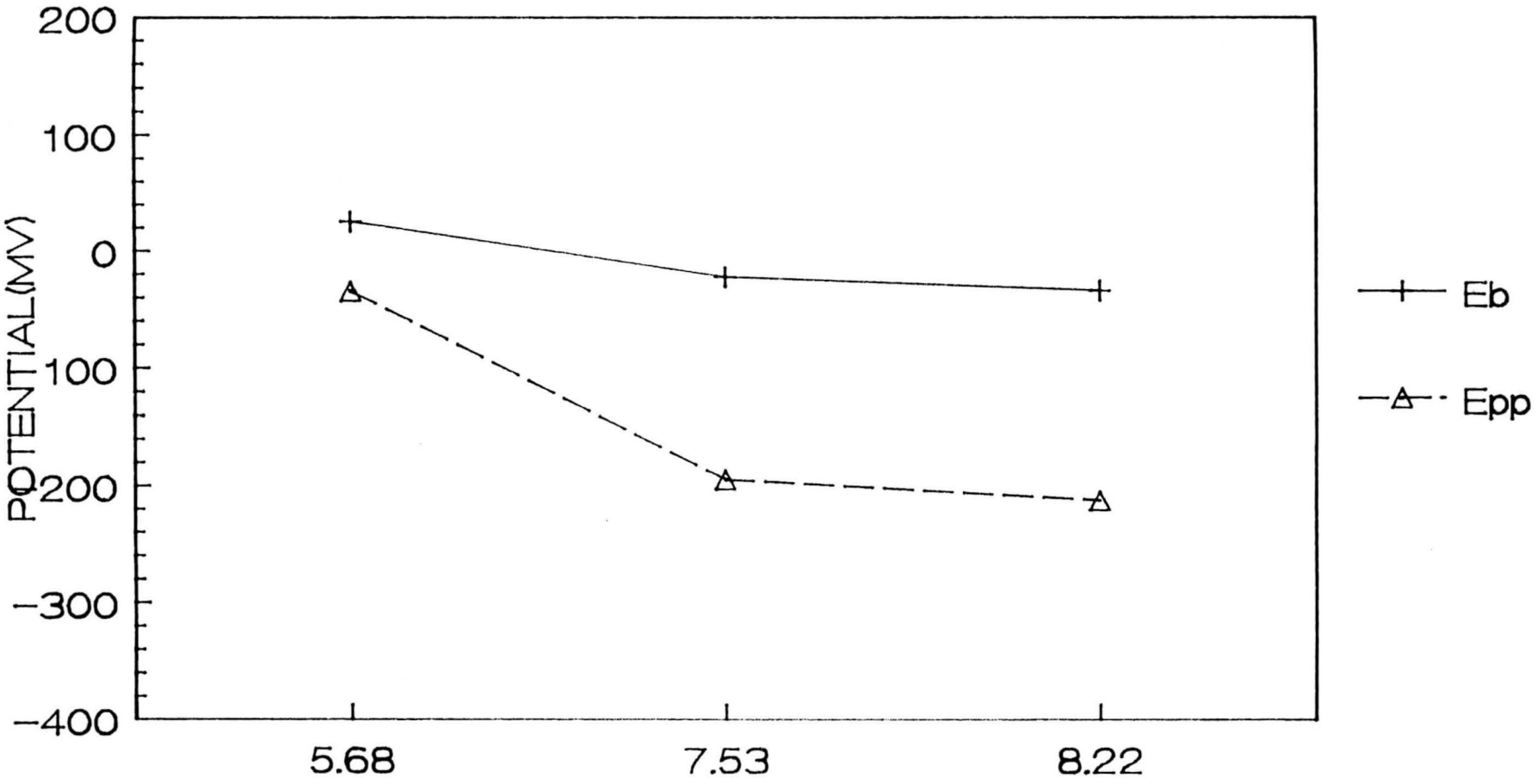

FIG.19 POTENTIAL VS. AL CONTENT
IN 100PPM NACL

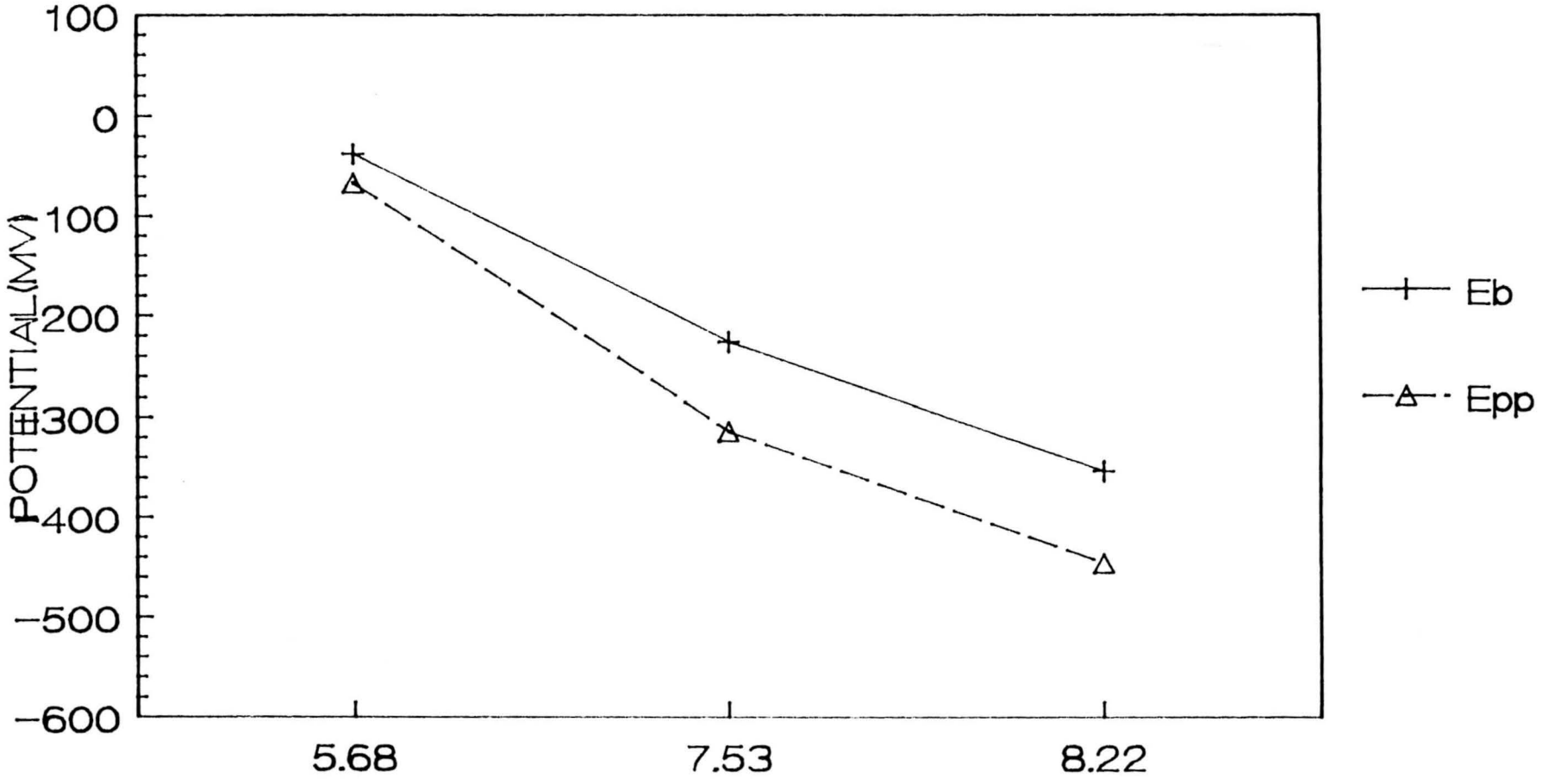

FIG.20 BREAKDOWN POTENTIAL VS AL CONTENT
IN 30PPM & 100PPM NACL

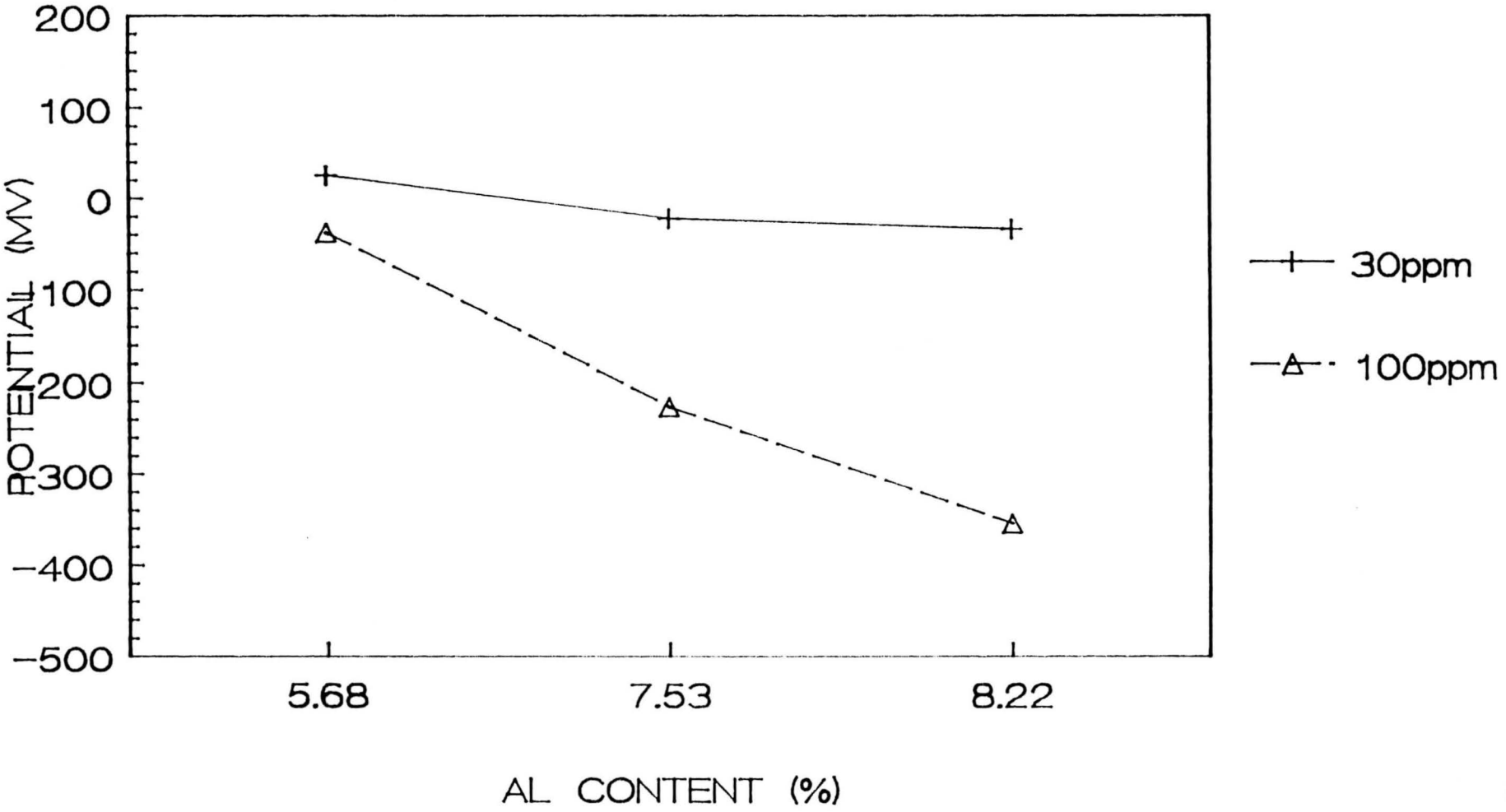

FIG.21 PRIMARY POTENTIAL VS AL CONTENT
IN 30PPM & 100PPM NACL

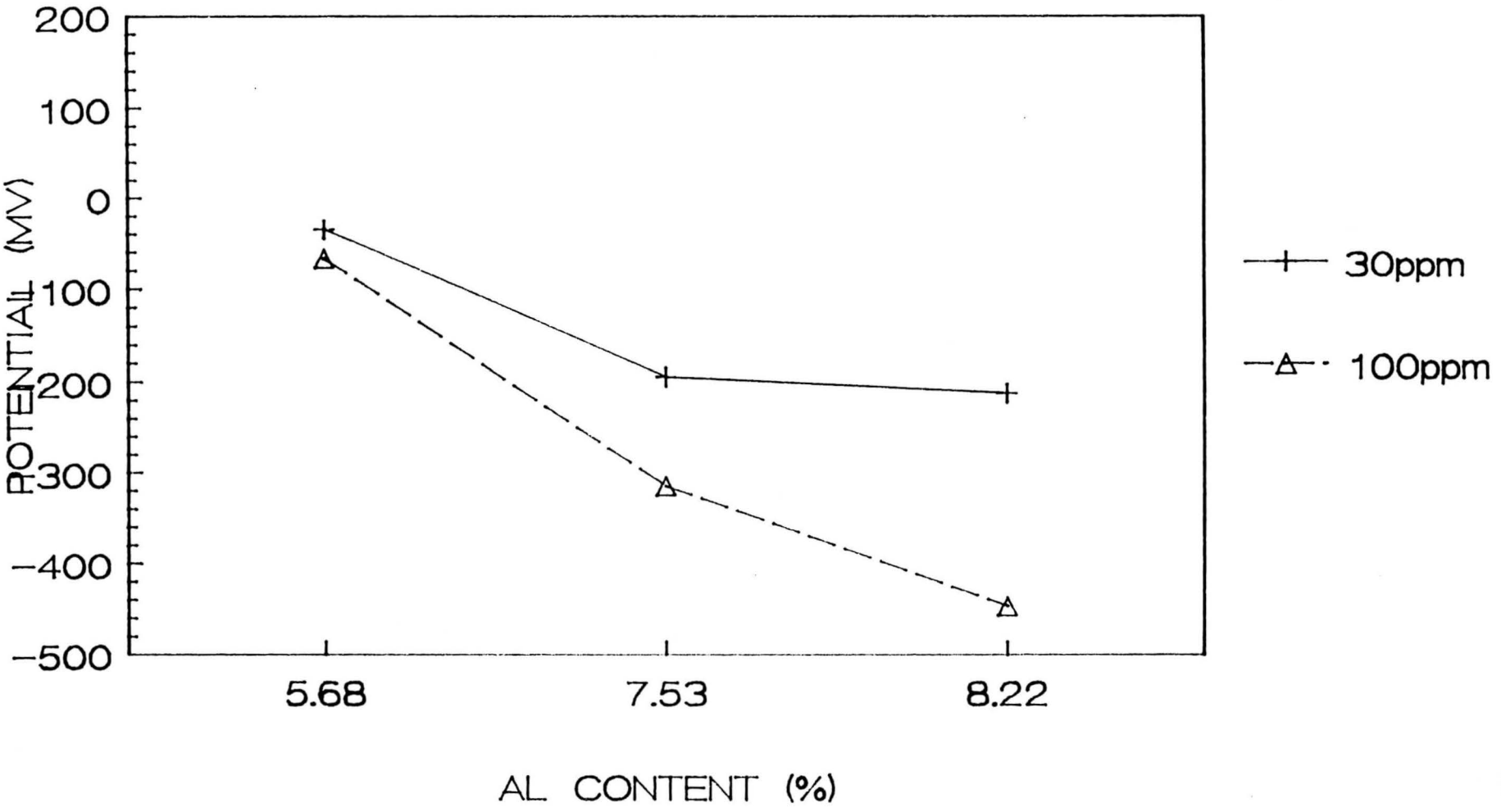

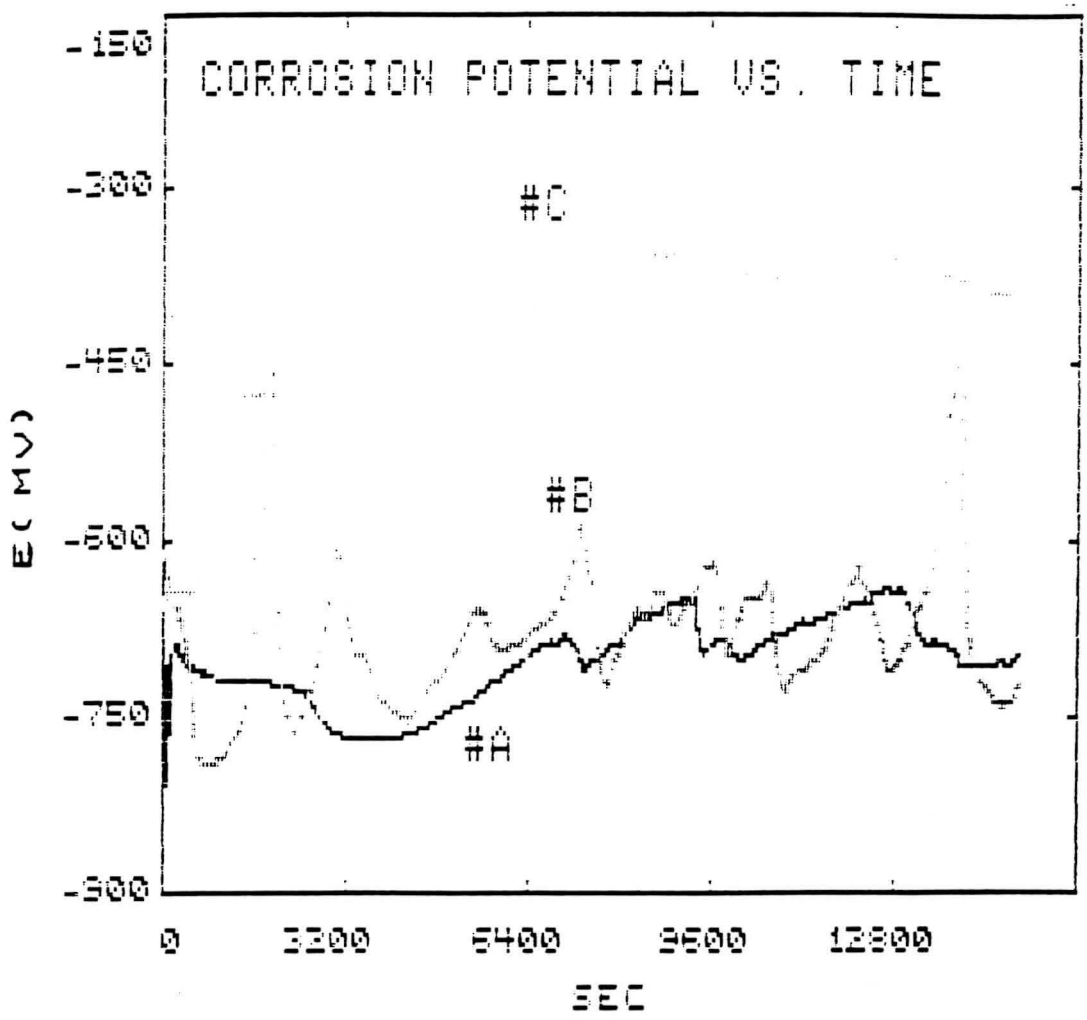

FIG. 22 Corrosion Potential Vs Al Content in 100 ppm NaCl Solution

FIG. 23 CORROSION RATE VS CURRENT DENSITY

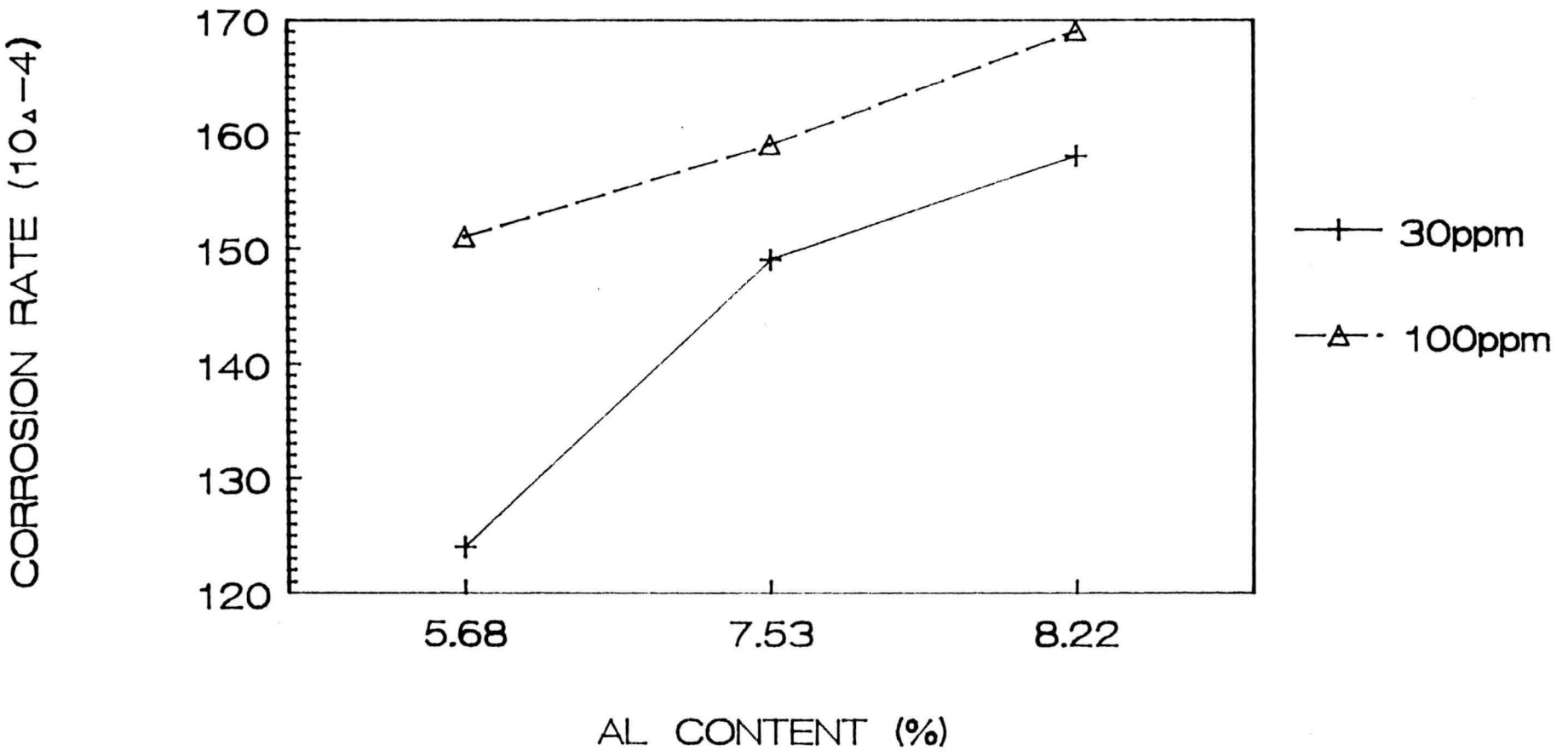

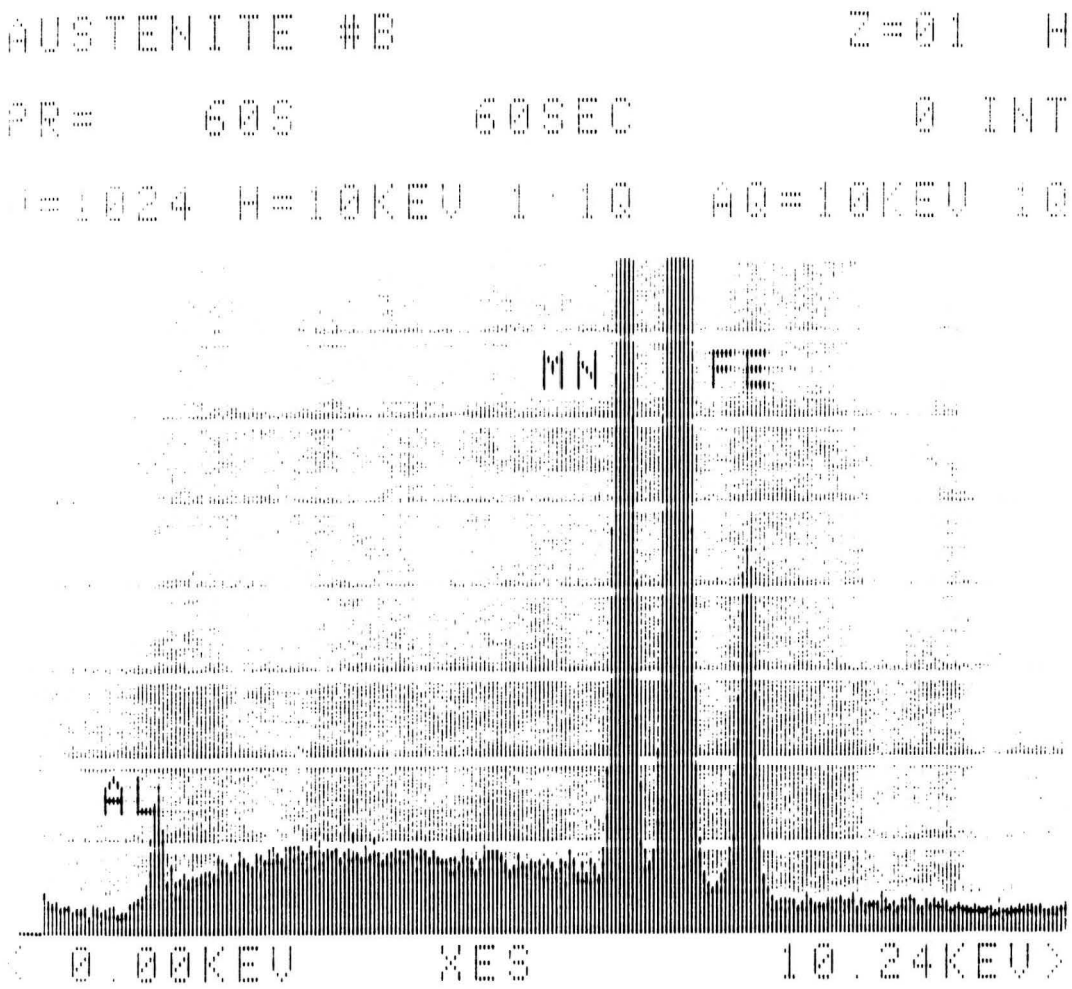

FIG. 24 EDS Analysis of Austenite in Alloy B Before Potentiodynamic Polarization

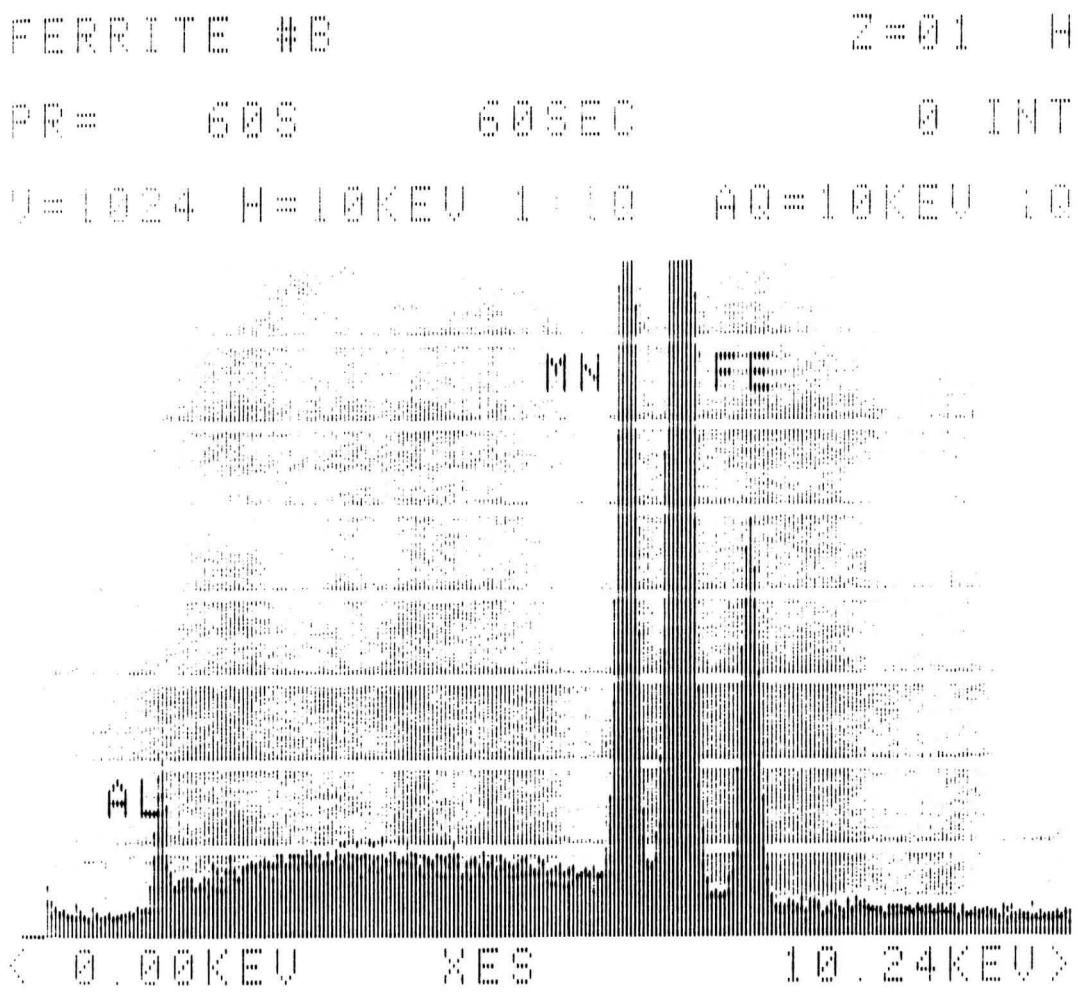

FIG. 25 EDS Analysis of Ferrite in Alloy B Before Potentiodynamic Polarization

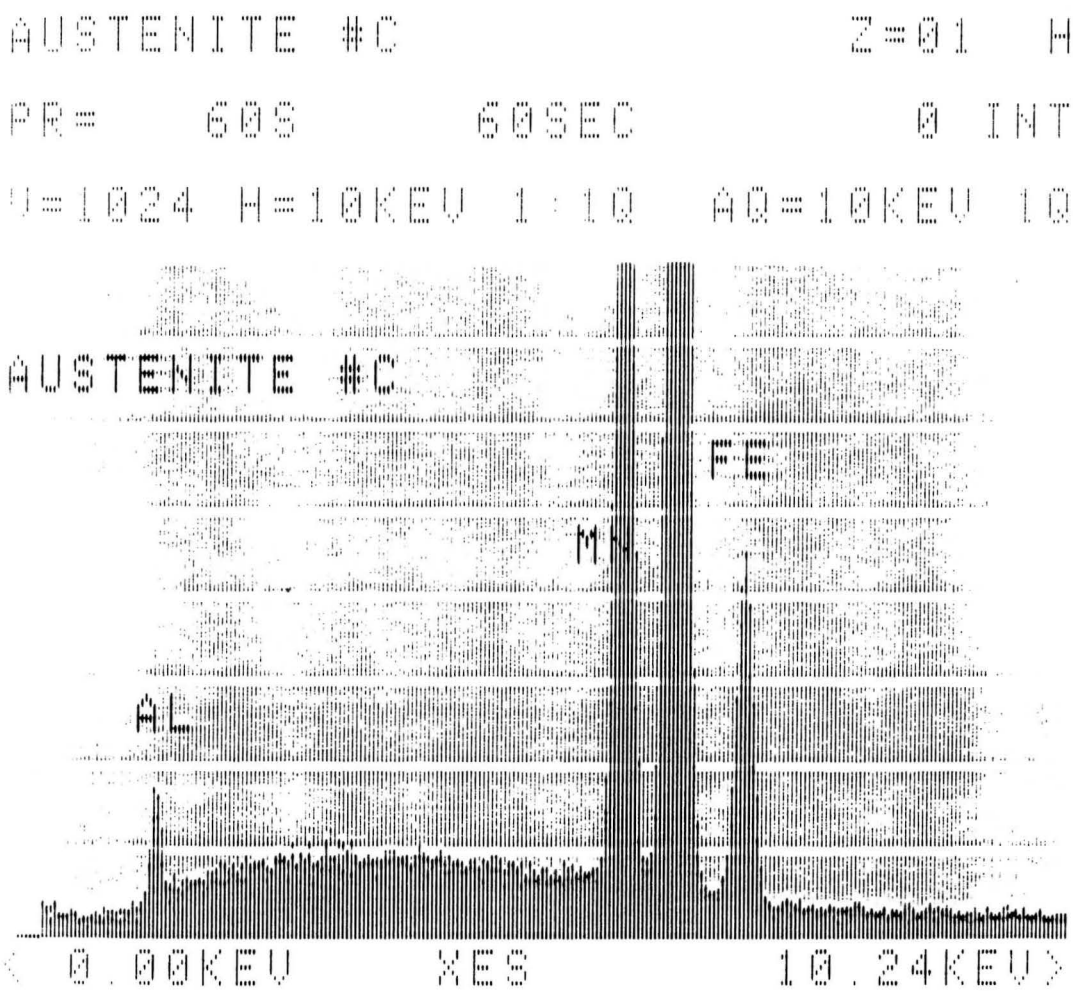

FIG. 26 EDS Analysis of Austenite in Alloy C Before Potentiodynamic Polarization

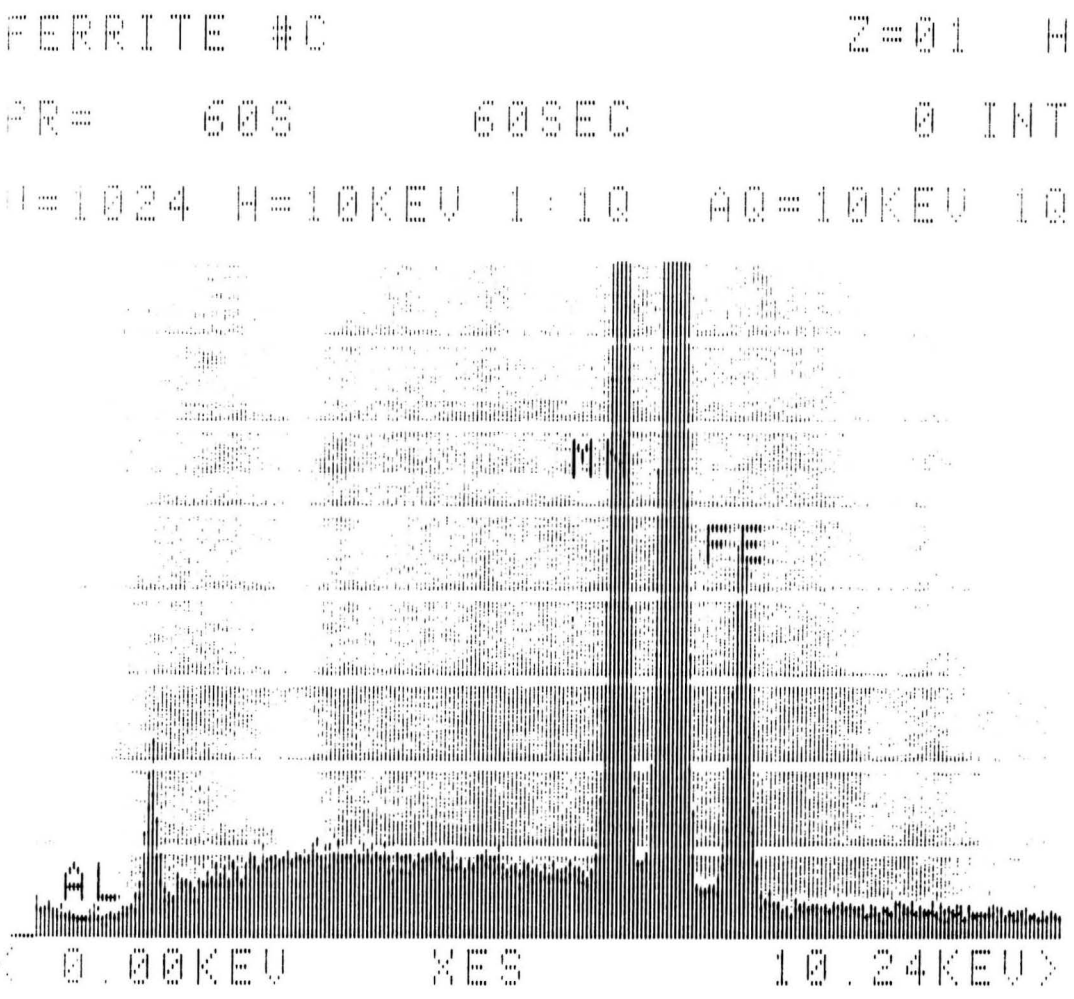

FIG. 27 EDS Analysis of Ferrite in Alloy C Before Potentiodynamic Polarization

APPENDIX A:

CHEMICAL CLEANING

CHEMICAL CLEANING

Dip in:	Chromic acid (CrO_3)	20 g
	Phosphoric acid (H_3PO_4)	50 ml
	Water to make	1 l
	Temperature	80 °C
	Time	until clean

APPENDIX B:

LIST OF SYMBOLS

LIST OF SYMBOLS

Symbol	Definition	Unit
α	Ferrite	None
r	Austenite	None
$K\alpha$	Characteristic Radiation of X-ray Tube	Å
ppm	Weight Percent	10^{-6}
E_b	Break Potential	mv
E_{pp}	Primary Potential	mv
E_{corr}	Corrosion Potential	mv
I_b	Breakdown Current Density	ua/cm^2
I_c	Critic Anodic Current Density	ua/cm^2
I_{corr}	Corrosion Current Density	ua/cm^2
R_w	Corrosion Rate	mm/yr

REFERENCES

1. W. Justusson, V. F. Zaky and E. R. Morgan, "The Mechanical Properties of Iron-Aluminum Alloys," Trans. ASM, Vol. 49, 1957, P. 905.
2. J. L. Ham and R. E. Cairns JR, "Manganese Joins Aluminum to Give Strong Stainless," Product Engineering, Vol. 29, No. 52, 1958, p. 50.
3. S. K. Banerji, "An Austenitic Stainless Steel Without Nickel and Chromium," Metal Progress, Vol. 113, No. 4, April 1978, P. 59.
4. J. Charles, A. Bergheran, A. Lutts and P. L. Dancoisne, "New Cryogenic Materials: Fe-Mn-Al Alloys," Metal Progress, May 1981, P.71.
5. G. L. Kayak, "Precipitation-Hardening Austenitic Alloys," Metal Science and Heat Treatment, 2, 1969, P. 95.
6. D. J. Schmatz, "Structure and Properties of Austenitic Alloys Containing Aluminum and Silicon," Trans. ASM, Vol. 52, 1960, p. 898.
7. R. S. Dean and C. T. Anderson, "Alloys," U. S. Patent No. 2, 329, 186, 14 September 1943.
8. R. Wang and H. Beck, "New Stainless Steel Without Nickel or Chromium for Marine Application," Metal Progress, March 1983, P. 72.

9. R. Wang and R. A. Rapp, "Seawater and H2SO4 Corrosion Studies of Several Ferritic Fe-Al Base Alloys," Proceedings of International Congress on Metallic Corrosion, Toronto, Canada, 3-7 June 1984, Vol. 4, P. 545.

10. R. Wang and R. A. Rapp, "Potentiodynamic Corrosion Behavior for Several Fe-Mn-Al Austenitic Steels," Proceeding of Conference: Trends in Critical Materials Requirements for Steels of the Future; Conservation and Substitution Technology for Chromium, Nashville, Tenn., October 1982.

11. Y. G. Kim, Y. S. Park, and J. K. Han, "Low Temperature Mechanical Behavior of Microalloyed and Controlled-Rolled Fe-Mn-Al-C-X Alloys," Metall. Trans., A, Vol. 16, 1985, P. 1689.

12. T. P. Perng and C. J. Altstetter, "Cracking Kinetics of Two-phase Stainless Steel Alloys in Hydrogen Gas," Metall. Trans., A, Vol. 19, 1988, p. 145.

13. S. C. Chang, J. Y. Liou, C. M. Wan and T. F. Liu, "The Corrosion Properties of Fe-Mn-Al Alloys," in Alternate Alloying for Environmental Resistance, G. R. Smolik and S. k. Banerji,(Eds) The Metallurgical Society, Warrendale, PA, 1986, P. 381.

14. Mars G. Fontana and Norbert D. Greene, Corrosion Engineering, 2nd, 1978, p.321.

15. Mars G. Fontana and Norbert D. Greene, Corrosion engineering, 2nd, 1978, p. 379.

16. S. C. Shih, Master Thesis, Tsing Hua University, Tsinchu, Taiwan, 1987.

17. Z. Szklarska-Smilowska, "Review of Literature on Pitting Corrosion Published Since 1960," Corrosion, June 1971, p.223.